USE OF SATELLITE IMAGERY FOR DEM EXTRACTION, LANSCAPE MODELING AND GIS APPLICATIONS

D. Poli, F. Remondino, C. Dolci

Institute of Geodesy and Photogrammetry, ETH Zurich, 8093 Zurich, Switzerland
(daniela, fabio, dolci)@geod.baug.ethz.ch

KEY WORDS: Pushbroom, ASTER, DEM, GIS, Visualization

ABSTRACT:

This paper describes a workflow for the DEM extraction from unrectified satellite stereo scenes, its visualization and integration in GIS environment. The results obtained using a stereo scene acquired by EOS-AM1/ASTER over Switzerland are presented and commented. The images are oriented with a rigorous photogrammetric model for CCD linear array sensors developed at IGP (ETH Zurich). The model estimates the sensor internal and external orientation with least squares adjustment, using a suitable number of ground control points. For the DEM generation, the points are automatically extracted in the images at sub-pixel accuracy with a least squares matching algorithm and their 3D coordinates are then calculated with forward intersection using the external and internal parameters estimated during the image orientation. The accuracy of the DEM was evaluated in three test areas using the DHM25 by Swisstopo as reference. The RMSE of the 3D distance between the recovered and reference terrain models is in the order of 1 pixel. After the surface generation, the terrain model is used for further investigations within a commercial GIS package. This includes not only the DEM analysis and comparison with already available geodata, but also the integration of cartographic information (i.e. existing vector features). The achieved results demonstrate the great potential of ASTER satellite imagery for geomatic applications at medium scales. Finally the DEM is imported in commercial software for a photo-realistic visualization.

1. INTRODUCTION

Today a large number of satellites provide imagery with high potential applications in various geomatic fields. Using stereo images with a favourable base over height ratio, a Digital Elevation Model (DEM) can be extracted and integrated in visualization packages or GIS environments for landscape representation and further analysis. Among the high resolution satellite images that have been successfully used for DEM generation and objects extraction we can mention IKONOS [Fraser et al., 2002; Kim et al., 2002; Toutin et al., 2003] and SPOT-5/HRG [Gruen et al., 2004]. If orthoimages are also generated or available, textured 3D models can be created and used for photo-realistic visualization.

In the last decades many efforts have been made in the development of satellite sensors capable to produce data for digital elevation models generation. One of the first constellations designed for this aim was the SPOT one, by CNES. The satellites (1-4) provided across-track stereo images of 10 and 20m ground resolution. DEMs with sub-pixel accuracy were extracted [Baltsavias et al., 1992, Gugan et al., 1988] and used for the first GIS applications [Welch, 1990]. Since then many new satellites have been launched, carrying sensors that can achieve less then 1m ground resolution (Quickbird). The largest part of the sensors currently in use for the acquisition of images for DEM generation flies along near-polar (to increase the ground coverage) and near-circular orbits and acquire along-track stereo images in a pushbroom mode. The main advantage of along-track stereo geometry with respect to the across-track one is that the time delay between the stereo images acquisition is smaller, reducing the land and cloud cover variations.

Today images with different spatial, radiometric, spectral and temporal resolutions are available on the market. The choice of the imagery mostly depends on the data availability for a specific location and time, on the price and the required scale of the application.

In particular, the imagery with 5 to 15m resolution (e.g. IRS-1C and 1D, SPOT-5/HRS, SPOT-2-4/HRV, ASTER) are suitable for mapping at 1:25000 up to 1:50,000 scale, have global coverage and in some cases are available at very low price. For example each ASTER scene costs 55 USD and contains 14 channels in the visible and infrared wavelength range, including two stereo channels for DEM generation.

The potentiality of these images for terrain mapping, vegetation and glaciers monitoring and other remote sensing applications is very high. For example DEM produced with ASTER data are used for the orthophotos generation from IKONOS images [Aniello, 2003] while, in Argentina, geological and thematic maps at different scales have been produced using ASTER images [Marin, 2002].

This paper describes our workflow for the DEM extraction from unrectified ASTER stereo scenes, its visualization and integration in a GIS environment. An evaluation concerning the accuracy of the recovered DEM is also presented.

2. DATASET DESCRIPTION

The Advanced Spaceborne Thermal Emission and Reflection Radiometer (ASTER) is one of the instruments carried on the EOS-AM1 platform, launched on December 18, 1999. ASTER is a cooperative effort between NASA and Japan's Ministry of Economy Trade and Industry (METI) formerly known as Ministry of International Trade and Industry (MITI), with the collaboration of scientific and industry organizations in both countries. The ASTER instrument covers a wide spectral region with 14 bands from the visible to the thermal infrared with high spatial, spectral and radiometric resolution. An additional backward looking near-infrared band provides stereo coverage. In details, ASTER consists of 3 downlooking sub-systems. The Visible and Near-infrared (VNIR) has three bands covering the

wavelength range 0.52-0.86µm (green, red, near-infrared), with a spatial resolution of 15m; the ShortWave Infrared (SWIR) has 6 bands in the range 1.6-2.4µm, with a spatial resolution of 30m; the Termal InfraRed (TIR) has 5 bands in the range 8.1-11.3µm, with a ground resolution of 90m. Each subsystem was built by a different Japanese company.

The instrument used for the DEM generation is the VNIR, the only one with stereo capability. It consists of two independent telescopes looking nadir and backward, with an angle of 27.6°. The backward looking telescope focal plane contains only a single detector array (channel 3B) and uses an interference filter for wavelength discrimination. The focal plane of the nadir telescope contains 3 linear arrays (channels 1, 2 and 3N) and uses a dichroic prism and interference filters for spectral separation, allowing all three bands to view the same area simultaneously. Channels 3N and 3B acquire in the same spectral range. The CCD lines for each band consist of 5000 detectors, but not all of them are active at one time. As during the time lag between the acquisition of the backward image and the nadir image the Earth rotation displaces the image center, the VNIR subsystem automatically extracts the correct 4100 pixels based on orbit position information supplied by the EOS platform. The detectors pixel size is different in the two telescopes. In the nadir one the size is 7.0µm x 7.0µm, while in the backward one it is 6.1µm x 6.1µm.

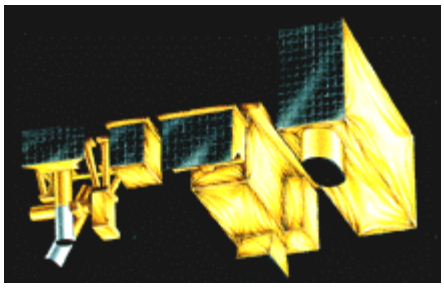

Figure 1. VNIR instrument.

The ASTER scenes are available at different processing levels, as described in [Abrams et al., 2002]. For our purposes, level 1A is used, because it is not georeferenced and reflects the original acquisition geometry. The scenes were acquired on 25th June 2003 at about 10:40 a.m. over Switzerland (orbit 18714, path 195, row 27). They cover an area of approximately 60km x 60km, centred in 47°09'43"N and 7°42'28"N (Figure 2).

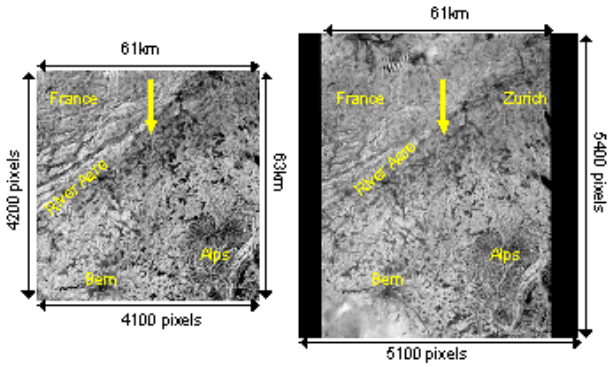

Figure 2. The ASTER images: 3N on the left, 3B on the right. The arrow indicates the flight direction.

3. DEM GENERATION

3.1 Preprocessing

The stereo images corresponding to bands 3N and 3B have been extracted from the original HDF file in IDL environment. They have different size: 4100 x 4200 pixels for 3N and 5100 x 5400 pixels for 3B. Due to the different detector size, the ground coverage in across-direction is the same. In along-track direction, the scene 3B covers a longer area than 3N (Figure 2). The original scenes have been radiometrically corrected using the coefficients contained in the HDF files in order to remove a vertical striping and other disturbing effects. Then a radiometric enhancement with Wallis filter was applied to facilitate the point matching (Figure 3).

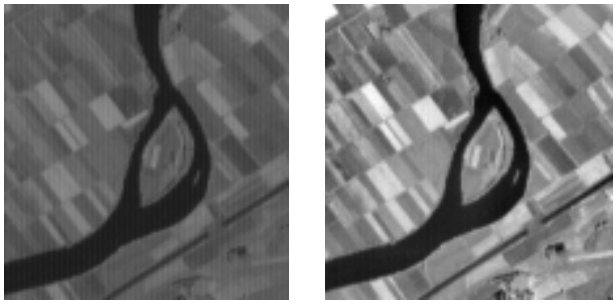

Figure 3. Zoom in the image before (right) and after (left) the radiometric correction and enhancement.

46 points have been measured in the images with template least-squares matching [Gruen, 1985] and their object coordinates have been read on 1:25,000 scale maps in the Swiss coordinate system (CH1903). The coordinates have been transformed into the fixed Cartesian geocentric system (later on called ECR). The points' location in the nadir image is shown in Figure 4.

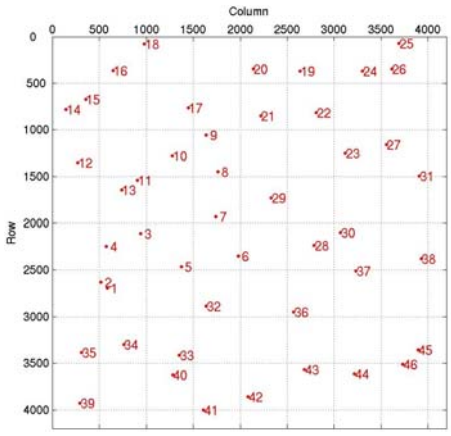

Figure 4. Distribution of 46 object points.

For the georeferencing of pushbroom imagery the position and attitude of the sensors at the acquisition time of each image line is required. The metadata contained in the HDF file supplied this information. The sensor position and velocity were available in ECR system correspondence of so-called lattice points with known time and position in the image. The acquisition time of each image line was computed with linear interpolation, assuming a constant scanning interval. From the position and velocity vectors, the attitude has been computed for each lattice point. Then the sensor position and attitude have been interpolated for each line with cubic splines.

3.2 Images orientation

The stereopair formed by the 3N and 3B images has been orientated using a rigorous sensor model developed at IGP and already applied to different linear scanners carried on satellite and aircraft (Poli, 2004). The model estimates the sensor internal and external orientation within a bundle adjustment, using a suitable number of well-distributed ground control points. The mathematical model is based on the collinearity equations, because each image line is the result of a nearly parallel projection in the flight direction and a perspective projection in the CCD line direction. In order to describe the acquisition geometry of the two-lens optical system contained in VNIR, the relative orientation (displacements and rotations) of the backward viewing lens with respect to a nadir one is introduced. The sensor position and attitude are modeled with piecewise 2nd order polynomial functions (PPM) depending on time. The internal orientation is modeled with additional parameters (APs), describing the systematic errors due to: principal point displacement (dx_P, dy_P), focal length variation (dc), radial symmetric (k_1, k_2) and decentering lens distortion (p_1, p_2), scale variation in CCD line direction (s_y) and the CCD line rotation in the focal plane (θ). The determinability of the APs is studied checking the correlation with the other APs, the TPs object coordinates and the PPM parameters. The functions modeling the external and the internal orientation are integrated into the collinearity equations, resulting in an indirect georeferencing model. Due to their non-linearity, the complete equations are linearized according to the first-order Taylor decomposition with respect to the unknown parameters. The resulting system is solved with a least-squares method, using well-distributed Ground Control Points (GCPs). The minimum number of GCPs depends on the total number of unknowns, according to the PPM and self-calibration configuration.

In order to process the ASTER/VNIR sensor, the software has been adapted in order to read stereo images with different size and CCD dimensions. The initial approximations for the PPM parameters were calculated from the ephemerides contained in the HDF files. Due to the lack of information, the initial approximations for the APs were set to zero. A group of the object points was used as GCPs and the remaining as tie points for final check (Check Points CPs). In the first tests the external orientation only was estimated, using different distributions of GCPs (8 and 12) and 2 and 4 segments for the PPM. For each test the external and internal accuracy of the system have been analyzed through the sigma naught a posteriori, the standard deviation and the RMSE of the CPs. Using the blunder detection included in the model and taking a threshold of 3.0 (critic value of t-Student distribution with infinite redundancy and a confidence interval of 99.9%), 8 points have been identified as outliers and eliminated, because they were rejected in the test in almost all configurations. After the blunder removal, the indirect georeferencing model was re-applied with the same GCPs and PPM configurations above described and with and without self-calibration. The results obtained using 2 and 4 segments for the PPM were quite similar. The RMSE of the CPs obtained without self-calibration were in the order of 1-2 pixels for almost all configurations, with theoretic values (sigma) of about 1 pixel and sigma naught a posteriori of 3.5-3.7μm. Using self-calibration, the bundle adjustment was run fixing the external orientation parameters to the values previously estimated without self-calibration and keeping the APs free. Different tests have been run to check the correlation between the APs and the ground coordinates of CPs and to decide which parameters had to be estimated. From this analysis, the most significant parameters were: k_1, k_2, p_1, p_2 and s_y. The maximum combined effect of this parameters (evaluated at the extremes of the image lines) was about 14μm (2.0 pixels) for 3N and 13μm (2.1 pixels) for 3B. As expected, the correction of the internal orientation parameters improved the internal and external accuracy of the adjustment. The results obtained with 4 segments in the PPM with 8 and 12 GCPs and with/without self-calibration are reported in Table 1.

Table 1. Results obtained using 4 segments in the PPM, without self-calibration (SC=N) and with self-calibration (SC=Y).

SC	GCP	CP	σ_0 (μm)	RMSE CPs (m)			σ CPs (m)		
				X	Y	Z	X	Y	Z
N	8	30	3.7	27.6	30.1	22.3	15.2	10.4	14.6
N	12	26	3.5	22.6	20.1	16.3	11.2	4.4	8.6
Y	8	30	1.1	13.6	14.8	14.4	7.0	3.5	5.8
Y	12	26	1.0	12.7	12.2	14.0	6.5	3.4	5.0

3.3 Matching and DEM generation

The image matching developed at IGP for images acquired by airborne or spaceborne linear array sensors was used [Zhang et al., 2003]. The algorithm, included in the SAT-PP software, is based on the Multi-Photo Geometrically Constraint (MPGC) matching algorithm [Gruen, 1985; Baltsavias, 1991] and combines feature point, edge and grid point matching. Sub-pixel accuracy can be achieved for all the matched features. Using the matching in unconstrained mode, about 1,800,000 points have been extracted without any external or internal orientation information. The 2D image coordinates of the homologous points have been transformed in a 3D point cloud in ECR system by forward intersection, using the external and internal orientation parameters estimated with the indirect georeferencing model. The geocentric coordinates have been transformed in the Swiss local system CH1903, for later comparisons. Then a 50m regular grid DEM (later on called ASTER-DEM) has been generated using a software available at IGP. The DEM is shown in Figure 5.

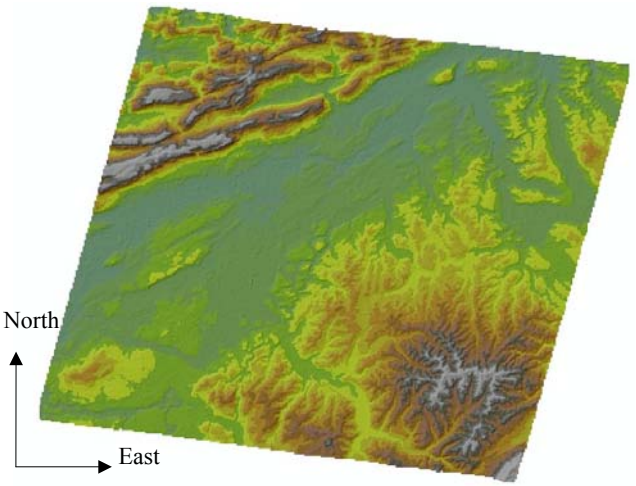

Figure 5. DEM generated from ASTER stereo images and displayed in colour coding mode, with a regular grid of 50m.

3.4 DEM evaluation accuracy

The accuracy of a DEM is usually represented by the spatial resolution (grid space) and the height accuracy and different

evaluation have been done [Ackermann, 1994; Takagi 1996, Kraus, 2004].
According to previous studies on the evaluation of DEM generated by ASTER, a vertical accuracy of approximately ±15m can be achieved [Hiranoa et al., 2003; Cuartero et al., 2004]. In our application, the DHM25 product of the Federal Office of Topography [Swisstopo, 2004] is used to estimate the accuracy of the generated DEM. The DHM25 is available for all Switzerland in blocks of about 17.5km x 12.0km. It is obtained from the Swiss National Maps at 1:25,000 scale, digitising contour lines and spot heights. The height accuracy of this product is around 2m (3m on the Alps). 20 blocks were overlapping the area covered by the ASTER scene, as shown in Figure 6.

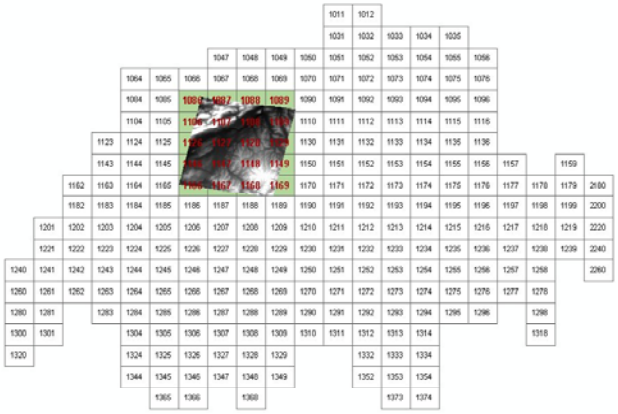

Figure 6. The 20 selected DHM25 blocks used as reference.

The comparison between the reference DHM25 and the ASTER-DEM has been made with the commercial software Geomagic Studio v.6 by Raindrop. Because of the great amount of data, among the 20 blocks, 3 blocks called 1107, 1128 and 1147, whose location is shown in Figure 7, are analyzed in details.
From each DHM25 block, provided as GRID file, a surface has been generated and compared to the overlapping part of the ASTER point cloud. The 3D Euclidean distance between the reference surface and the recovered point cloud is taken into account for the analysis. As output, the software gives the number of points compared (N), the minimum, maximum and mean distance (Min, Max, Mean) and the standard deviation (STD). From this data the RMSE is computed. The results obtained for each block with the measured DEM are reported in Table 2 and the error distribution is visually represented in the first column of Table 3.

Table 2. Comparison between the ASTER-DEM and the reference DEMs.

DEM*	N	Min [m]	Max [m]	Mean [m]	STD [m]	RMSE [m]
1107	112326	-84.49	67.89	-7.58	16.68	18.32
1128	127228	-54.51	55.82	-3.73	14.15	14.63
1147	136508	-66.52	60.77	-10.37	15.27	18.46

**reference DHM25 from Swiss Federal Office of Topography*

For the analyzed blocks the mean values are smaller than 1 pixel, while the RMSE and standard deviations are slightly larger than 1 pixel. Anyway it must be taken into account that the areas covered by trees may cause large errors. In fact, the reference DEMs are produced digitising the contour lines of 1:25,000 scale maps and represent the form of the surface without vegetation and buildings. On the other hand, the generated 3D point cloud does not represent always the real terrain, but the surface imaged from the satellite sensor. If the forest areas are removed, we expect a reduction of the differences mean values and a slight improvement in the standard deviations and RMSE, as already proved in [Poli et al., 2004].

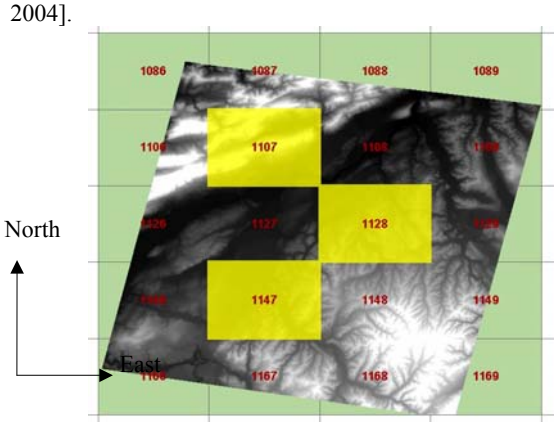

Figure 7. Location of the three areas used for the accuracy analysis.

4. GIS APPLICATIONS

The 3D data recovered by photogrammetric techniques was imported in GIS environment for further analysis and visualisation. Vector and raster data describing the topography, landcover and land use of the terrain can be overlaid on the DEM in order to obtained a 3D combined model. The incorporation of elevation and terrain data can improve the information extraction for example, in discriminating wetlands, flood mapping, and forest management. Among the packages available on the market, we used ArcGIS 8.3 (ESRI), in particular ArcScene desktop application available with the 3D Analyst extension. Using ArcScene it is possible to create 3D maps for visualization and rendering. ArcScene cannot perform real-time rendering of big data sets and has a static level of detail control.
In the following different GIS applications with the recovered ASTER-DEM are reported.
The first application was the assessment of the ASTER-DEM quality by comparing the height difference with respect to the reference ones from Swisstopo. The analysis has been done again on the blocks named 1107, 1128 and 1147, consistently with the analysis in Section 3.4. The planimetric distributions of the height differences, together with the histograms of the height differences, are reported in the second and third columns of Table 3. The errors distribution is very similar to the ones obtained in the previous analysis, confirming an accuracy around 1 pixel.
In order to verify the influence of the trees in our results, the land use layer (vector data at 1:200,000 scale by Swisstopo) has been overlapped on the DEM. From Figure 9 it can be noticed that the areas classified as forest and the areas with positive differences between the two surfaces (i.e. ASTER-DEM higher that reference DEM) have the same clustering.

Table 3. Results of the comparison of the three reference areas (from top to bottom: 1107, 1128, 1147). First column: errors distribution between 3D point cloud and reference DEM (Geomatic Studio). Second column: errors distribution between measured DEM and reference DEM (ArcGIS). Third column: histogram of the height differences frequency (ArcGIS)

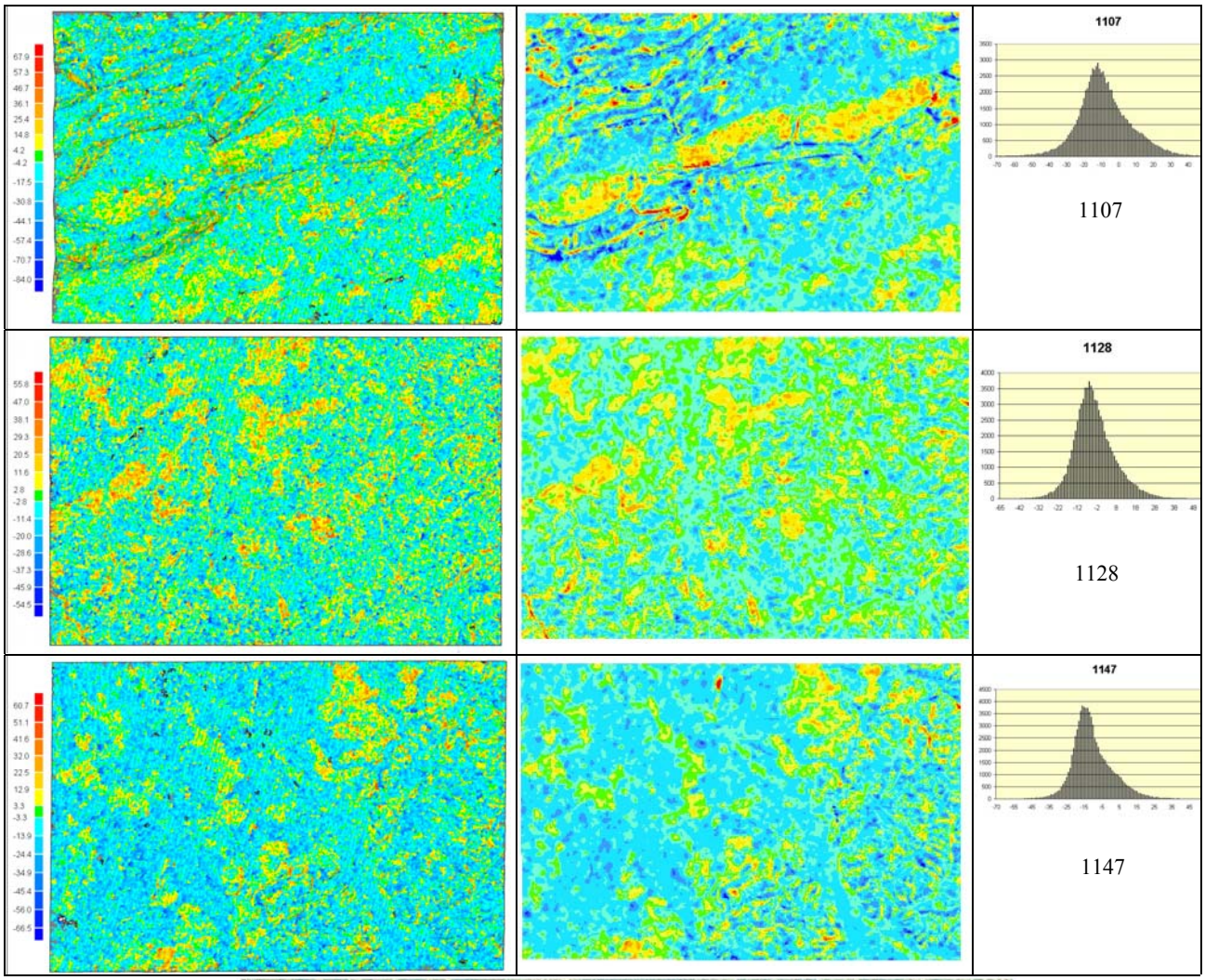

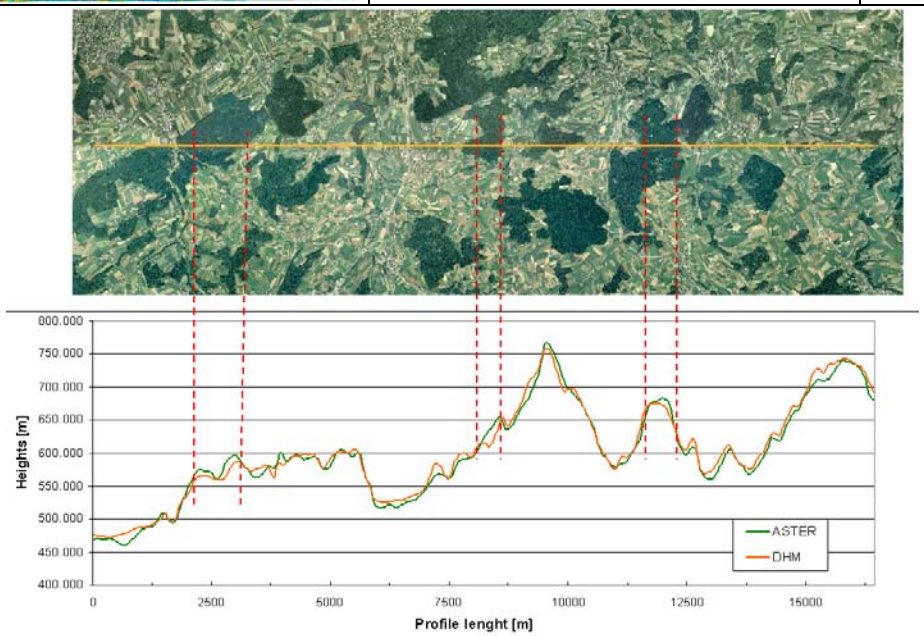

Figure 8. Analysis of a section profile in area 1128. Top: section location in the orthoimage; bottom: height profile for the ASTER-DEM (green) and the reference DEM (orange).

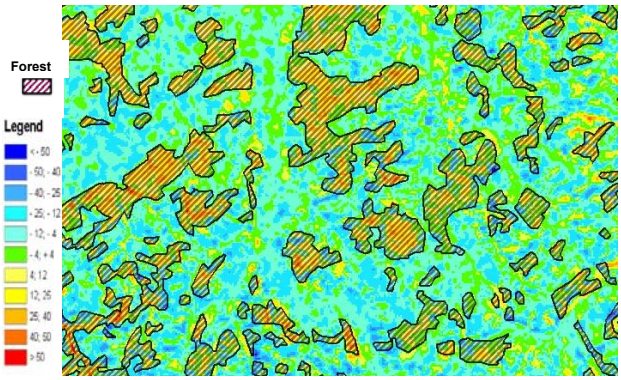

Figure 9. Positive errors areas corresponding with forest areas (reference area n.1128).

The presence of trees in areas with positive errors is also confirmed by the visual and qualitative comparison with an orthophoto of the same area. The orthophotos were generated by Swisstopo in 1998, with a spatial resolution of 0.5m. For this analysis the height profiles of the ASTER-DEM and the reference DEM along a section have been plotted and compared. Figure 8 shows the location of the section (orange line) in the orthoimage and the plot of the height profiles. Considering the profiles plotting, it can be noticed that the section segments where the ASTER-DEM profile is higher than the reference one corresponds to areas covered by trees in the orthoimage. In the rest of the section the fitting is quite good.

The terrain's slopes have been also calculated and represented, as shown in Figure 10. Slopes are useful information for many morphological studies and can be employed e.g. for debris flows hazard maps.

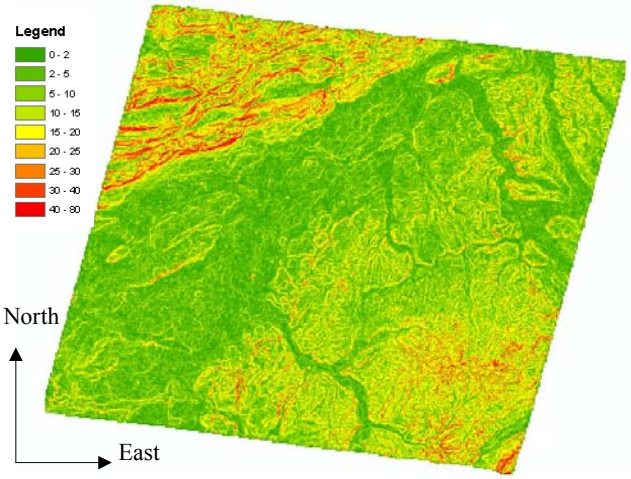

Figure 10. Representation of DEM slopes (in degrees).

The cartographic information, available as a vector data at 1:200,000 scale by Swisstopo, describing the hydrography and the settlement coverage was finally imported and visualised on top of the DEM. Figure 11 shows the two layers over the DEM in hillshaded mode. The fitting between the DEM and the other layers is quite good, confirming the correctness of the recovered DEM and the potential of the ASTER-DEM as terrain support for land cover analysis.

5. 3D VISUALIZATION

Viewing data in three dimensions gives new perspectives about the derived data, adding insights that would not be readily apparent from a planimetric view. Having multiple viewpoints

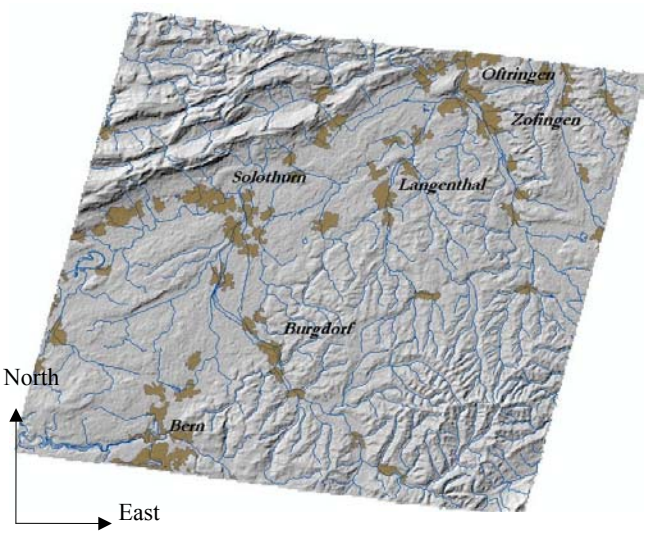

Figure 11. ASTER-DEM in hillshaded mode with settlement (brown) and hydrography (blue) layers.

of the data guarantees to have a first raw exploration of their quality.

The ASTER-DEM has been imported in the commercial package Erdas Imagine 8.7 for 3D visualization. Erdas, and in particular Virtual GIS, allows the management and visualization of geographic data, for interactive fly-through of user-defined flight paths. The user can also drape multiple GIS layers and raster data, even if some aliasing effects are present in the produced video animations. Furthermore the package allows high-resolution rendering of screenshots, anaglyph stereo viewing, static level of detail control and VRML 2.0 support. For the photo-realistic visualization of the measured DEM, an orthoimage of the ASTER scene has been generated with PCI Geomatica software, using as reference DEM the measured one and as original image a combination of the bands 1, 2 and 3N of the VNIR instrument (corresponding to the green, red and near infrared channels). The resulting false-colour rectified image can also be used for further landscape and vegetation analysis.

The ASTER-DEM was imported in Erdas after the conversion in the internal file format (IMG), which has a considerably reduced file size. Afterwards, different raster information has been overlapped: the available orthoimages from Swisstopo (Figure 12) and the generated ASTER orthoimage (Figure 13).

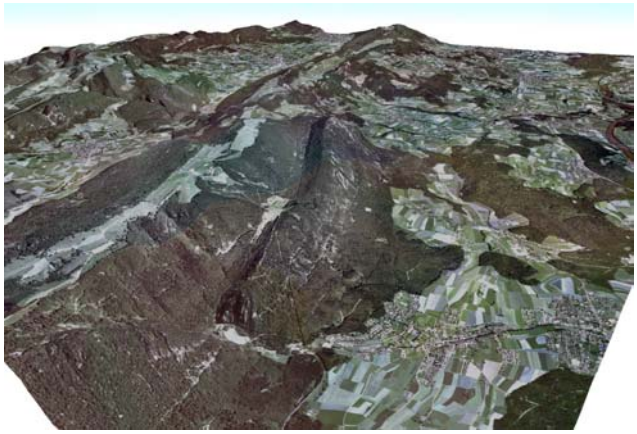

Figure 12. 3D texture model of ASTER-DEM with the Swisstopo true-colour orthoimages

It can be noticed that the 0.5m spatial resolution orthophoto fit quite well on the recovered ASTER-DEM, adding a very nice photo-realistic visualization of the analysed area.

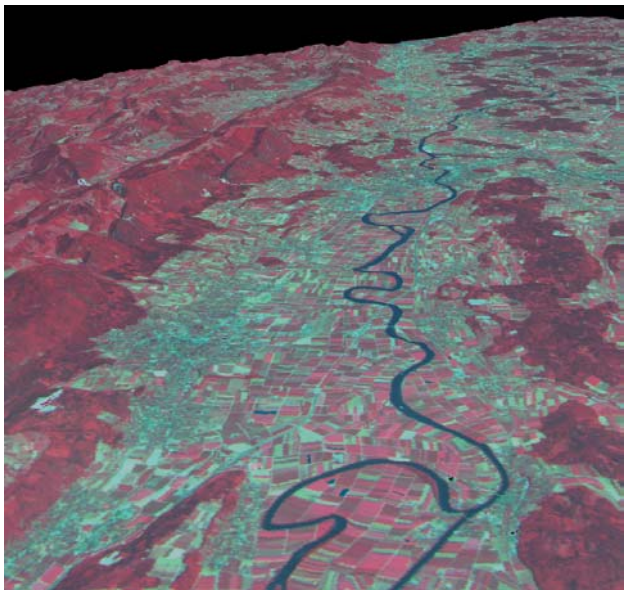

Figure 13. A view of the 3D texture model of ASTER-DEM with the ASTER false-colour orthoimage.

6. CONCLUSIONS

In this paper the potentials of middle resolution satellite images for the generation of DEM and its use in Geographyc Information Systems (GIS) has been verified using the Advanced Spaceborne Thermal Emission and Reflection Radiometer (ASTER) on board the NASA's satellite Terra. A stereopair from ASTER-VNIR sensor (15m ground resolution) acquired on 25th June, 2003 over Switzerland was used for our tests. The processing for DEM generation included the radiometric pre-processing of the stereo images (channels 3N and 3B, infrared band), the object points measurement, the sensor orientation with a rigorous sensor model developed at IGP for pushbroom sensors, the points extraction with unconstrained least-squares matching and the 3D coordinates calculation with forward intersection. The accuracy of the resulting point cloud has been evaluated comparing the 3D distance between each point of the generated point cloud and the surface generated from the DHM25 vector by Swisstopo (1-3m accuracy). For the analyzed test sites (three 17.5km x 12.0km blocks) the mean values are smaller than 1 pixel, while the RMSE and standard deviations are slightly larger than 1 pixel. As the reference DEMs represent the form of the surface without vegetation and buildings, while the generated 3D point cloud represents the surface imaged from the satellite sensor, the effect of the trees on our results have been evaluated in a further analysis. From the point cloud a regular 50m x 50m grid space DEM was generated and imported in ArcGIS. The ASTER-DEM was firstly compared to the reference DHM25 through their height differences, than the land use layer (vector data at 1:200,000 scale by Swisstopo) was overlapped on the height difference layer. As expected, the areas classified as forest and the areas with positive differences between the two surfaces had the same clustering. Using the ASTER-DEM further analysis of the terrain can be performed. As an example, the cartographic information describing the water and settlement coverage has been overlaid.

For 3D visualisation, Erdas software was used. In order to improve the rendering, a false colour orthophoto was generated from the ASTER images and mapped onto the DEM.
In conclusion, the ASTER scenes, available at very low price (55$ each), represent a very convenient and reliable data for the DEM generation and land analysis at 1:25,000 up to 1:50,000 scale. The correctness of the recovered DEM has been verified with different analysis. DEM generated using middle resolution satellite imagery can be used not only for landscape visualisation, but also for the terrain coverage/use monitoring. Furthermore, using multi-temporal scenes, changes in the vegetation, water coverage or glaciers extend can be monitored with relatively few costs and good accuracy.

AKNOWLEDGMENTS

The authors would like to thank Natalia Vassilieva for her help in the point measurement.

REFERENCES

Abrams, M., Hook, S., 2002. ASTER User HandBook. Available at http://asterweb.jpl.nasa.gov/documents/ (last visited: October 2004).

Ackermann, 1994. Digital Elevation Models - Techniques and Applications, Quality Standards, Development. IAPRS, Vol. 30, Part 4, pp 421-432.

Aniello, P., 2003. Using ASTER DEMS to produce IKONOS orthophotos. Available at:
http://www.spaceimaging.com/whitepapers_pdfs/2003/pa_eom_paper_for_pdf.pdf

Baltsavias, E. P., 1991. Multiphoto geometrically constrained matching. Ph. D. dissertation, Institute of Geodesy and Photogrammetry, ETH Zürich, Mitteilungen No. 49.

Baltsavias E. P., Stallmann D., 1992. From Satellite Images to GIS with Digital Photogrammetry Using SPOT Data. In Proc. of EGIS 92, 23.-26. March, Munich, Germany, Vol. 2, pp. 945 - 946.

Cuartero A., Felicísimo A.M., Ariza, F.J., 2004. Accuracy of DEM genaration from Terra-Aster stereo data. IAPRS&SIS, Vol. 35, Part B6, pp. 225-260.

Fraser, C., Baltsavias, E.P., Gruen, A., 2002. Processing of Ikonos imagery for sub-metre 3D positioning and building extraction. P&RS, 56(3), pp. 177-194.

Gruen, A., 1985: Adaptive Least Squares Correlation: A powerful Image Matching Technique. South Africa Journal of Photogrammetry, Remote Sensing and Cartography, 14 (3), pp. 175-187.

Gruen, A., Remondino, F., Zhang, L., 2004. 3D modeling and visualization of large cultural heritage sites at very high resolution: the Bamiyan valley and its standing Buddhas. IAPRS&SIS, Vol. 35, Part B5.

Gugan, D.G., Dowman, I.J., 1988. Accuracy and Completeness of Topographic Mapping from SPOT Imagery. Photogrammetric Record, 12 (72), pp.787-796.

Hiranoa, A., Welcha, R., Lang, H., 2003. Mapping from ASTER stereo image data: DEM validation and accuracy assessment. ISPRS Journal, 57(5-6), pp 356-370.

Kim, T., Im, Y.J., 2002. Automated DEM extraction of urban areas from multi resolution satellite images. IAPRS&SIS, Vol. XXXIV, Part B2, pp. 223-227.

Kraus, K., Briese, C., Attwenger, M., Pfeifer, N., 2004. Quality measures for digital terrain models. Commemorative Volume for the 60th birthday of Prof. Dr. Armin Gruen, pp. 163-168.

Marín, G., 2002. GEOSAT-AR: Technology transfer program of ASTER data, image processing and applications. IAPRS&SIS, Vol XXIV Part B6. Available at http://www.isprs.org/commission6/proceedings/

Poli, D., 2004. Orientation of satellite and airborne imagery from multi-line pushbroom sensors with a rigorous sensor model. IAPRS&SIS, Vol. 35, Part B1, pp.130-135.

Poli, D., Zhang, L., Gruen, A., 2004. SPOT-5/HRS stereo images orientation and automated DEM generation. IAPRS&SIS, Vol. 35, Part B1, pp.421-432.

Swisstopo, 2004. http://www.swisstopo.ch

Takagi, M., 1996. A study of DEM accuracy according to spatial resolution. Proceedings of the 17th Asian Conference on Remote Sensing, on CDROM.

Toutin,T., Chénier, R., Carbonneau, Y., 2003. 3D geometric modelling of IKONOS Geo images. Proceedings of ISPRS Workshop "High Resolution Mapping from Space 2003", Hannover. Proceedings on CD.

Welch, R., 1990. 3-D terrain modeling for GIS applications. GIS World 3 (5), 26–30.

Zhang L., Gruen, A., 2003. Automatic DSM Generation from StarImager (SI) Data. 6th Conference on Optical 3-D Measurement Techniques, Vol.1, pp. 93-105.